MAPPING AND DETECTING CHANGES OF MANGROVE OVER CHINA FROM 1996 TO 2018 WITH JERS-1, PALSAR AND PALSAR2

Yuhan Zheng, Wataru Takeuchi

Institute of Industrial Science, the University of Tokyo, Tokyo, 1538505, Japan
Email: yuhan@g.ecc.u-tokyo.ac.jp; uiis.wataru@g.ecc.u-tokyo.ac.jp

KEY WORDS: mangrove; classification; change detection; ALOS PALSAR

ABSTRACT: Mangroves in China have experienced various changes in different time periods due to anthropogenic disturbances, climate change and national restoration policy. However, few studies quantitatively analyzed their extents and distribution changes. This study mapped and detected the changes of mangroves from 1996 to 2018 at the national scale. Firstly, a 2018 mangrove baseline was classified for the whole coastal China using ALOS PALSAR-2 and Landsat 8 composite imagery within a Random Forests Classifier. The mangrove base map has an overall accuracy greater than 95% and a kappa coefficient of 0.8858. Then a combination of map-to-image method and image-to-image method was created to detect the mangrove changes in the period 1996-2018, 2007-2018 and 2010-2018 using Normalized Difference Vegetation Index (NDVI) and Land Surface Water Index (LSWI) and HH band. This study demonstrated that the total areas of China's mangroves in 1996, 2007, 2010 and 2018 were 19,420 ha, 24,684 ha, 25,572 ha and 26,553 ha respectively. More than 90% mangroves were distributed in Guangdong province, Guangxi province and Hainan province. Mangroves in most areas kept increasing from 1996 to 2018 mainly due to the national conservation actions. The largest change observed was in Guangdong province where 4249.35 ha of mangrove gain occurred in the past 20 years. Changes in local mangrove extent were the consequence of both climate and anthropogenic drivers. These updated maps are of importance to the sustainable management and ecological assessments of mangrove ecosystems in China.

1. INTRODUCTION

Mangroves growing up in the intertidal area, provide a wide range of essential ecosystem services. They can serve as a nursery for juvenile coral reef fishes of many species (Nagelkerken et al., 2000), and protect the coastal zone against erosion and storms (Arkema et al., 2013). What's more, mangroves are also an important sink for carbon and play a great role in blue carbon ecosystems (Duarte et al., 2013). Murray et al. (2011) estimates that mangroves sequester 34.5-38.2 billion tonnes CO2 with an average carbon fixation rate of 5.98 tonnes CO2/ha/yr, which can contribute a lot to mitigating climate change and achieving sustainable development goals (Duarte et al., 2013). However, mangrove ecosystem is amongst the most vulnerable and threatened ecosystems in the world and has experienced a dramatic loss due to human population growth and coastal zone development. It has been reported that more than 50% of mangrove forests were lost globally since the 1980s (Spalding et al., 1997; Hamilton and Casey, 2016). International programs, such as Reduce Emission from Deforestation and Degradation (REDD+) and Kyoto Protocol, highlight the significance of immediate protection and conservation to prevent the further loss of mangrove. China only makes up about 0.14% of the world's mangrove area, but it holds one third of the world's mangrove species (Wang, 2007). However, mangroves in China experienced a 50% loss, from 40,000 ha in 1957 down to 18,800 ha in the mid-1980s (He and Zhang, 2001). Thus, it is of great importance to protect and recover the mangrove ecosystems in China.

Remote sensing (RS) technology provides a way to monitor the spatiotemporal distribution and health status of mangrove ecosystems, which helps us manage and protect them. To date, several global mangrove forest maps have been produced, such as The World Atlas of Mangrove (Spalding et al., 2010), Mangrove Forests of the World (Giri et al., 2011), and Global Database of Continuous Mangrove Forest Cover for the 21st Century (Hamilton and Casey, 2016). However, these mangrove forest maps are incomplete or outdated and may not reflect the latest spatial distribution of mangrove forests in China. Thus, in recent years, many researchers in China started to map the mangrove forests at a national scale. Wu et al. (2013) mapped the mangrove forest ecosystems in China for the 1990s, 2000s, and 2010s by visual interpretation of Landsat imagery. Jia et al. (2014) applied the object-based method to generate the mangrove forest maps and evaluated the effectiveness of conservation on mangroves in China (Jia et al., 2016). Combining the Landsat 7/8 and Sentinel-1A images, Chen et al., (2017) created a mangrove forest map of China in 2015 with high accuracy in Google Earth Engine (GEE) platform. Hu et al. (2018) monitored the mangrove forest changes in China between 1990 and 2015 through Landsat-derived spectral-temporal variability metrics. Although these studies gave an overview of the mangrove forests in China, the long-term holistic views of China's mangrove distributions are not completed. Jia et al. (2018) quantified the mangrove forests dynamics from 1973 to 2015 based on Landsat imagery which provided the first dataset of long-term China's mangrove distribution. However, due to the cloud influence, some areas entirely or partially lacked available images. Therefore, the results of their

research are not comprehensive. Synthetic Aperture Radar (SAR) images are not influenced by weather conditions and can reflect the structure information of mangroves which could help distinguish them with other vegetations. Thus, the combination of optical and SAR images would improve the accuracy and reliability of mangrove dynamics dataset.

The main objectives of this study are to 1) create the baseline of mangrove distributions in China with high accuracy; 2) establish the new long-term China's mangrove dynamics based on Landsat and ALOS PALSAR imageries.

2. MATERIALS AND METHODS

2.1 Study Area

Natural mangroves in China are distributed from Yulin Port, Hainan province (18° 9′ N) to Fuding, Fujian province (27° 20′ N), while planted mangroves have extended to Leqing Bay in Zhejiang province (28° 25′ N) (Wu et al., 2013). The study area (Figure 1) included mangroves in the whole coastal zone of China, encompassing five coastal provinces (Hainan, Guangxi, Guangdong, Fujian, and Zhejiang), Hong Kong Special Administrative Region, Macao Special Administrative Region and Taiwan.

2.2 Data

2.2.1 Remote Sensing Imagery: JAXA L-band SAR mosaics from JERS-1 for 1996 were downloaded from JAXA (JAXA EORC mosaic: http://www.eorc.jaxa.jp/ALOS/en/palsar_fnf/fnf_index.htm) and ALOS PALSAR mosaics for 2007, 2010 and 2018 were obtained in GEE. A Lee filter was used to filter the ALOS PALSAR bands to reduce the speckle effects (Lee, 1980). The SAR data was in digital number and need to be converted to sigma nought backscattering coefficient using Equation (1), with a calibration factor (CF) of -83 for ALOS PALSAR-2 and -84.66 for JERS-1. All SAR mosaics were resampled to 30 m resolution.

$$\sigma^o = 10 \times \log_{10}(DN^2) - CF \quad (1)$$

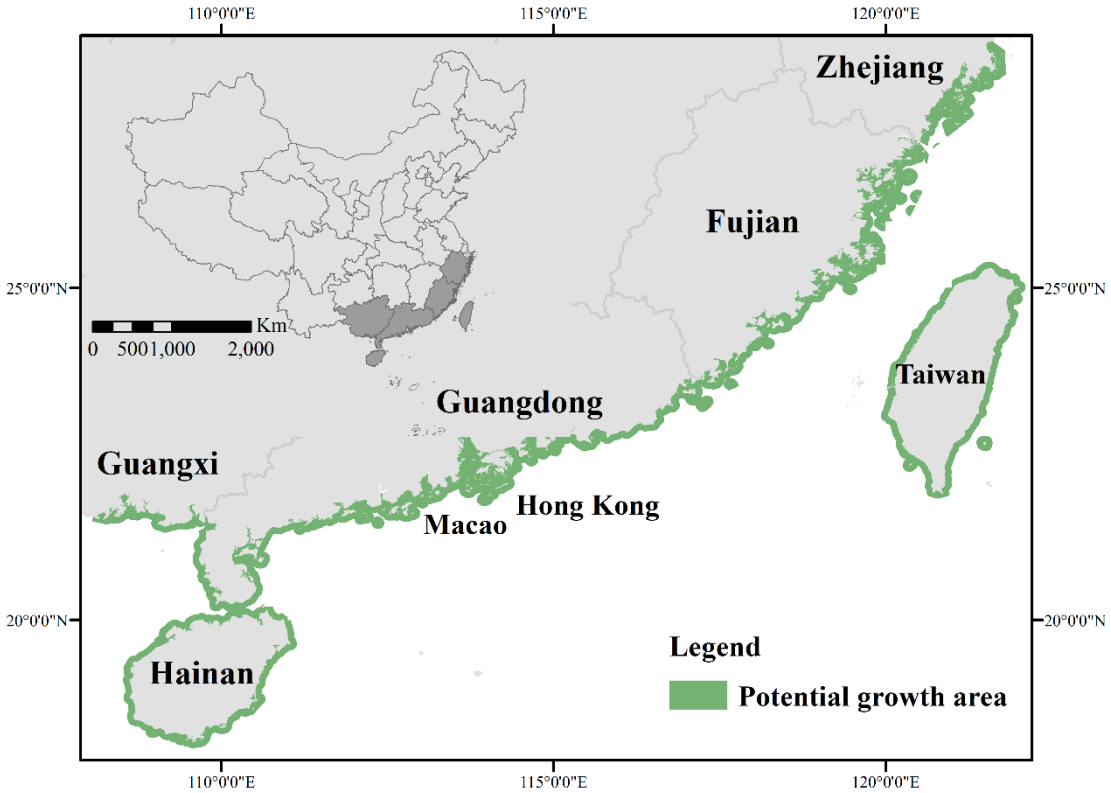

Figure 1 Location of study area and potential mangrove growth area in the whole coastal zone of China

Landsat 5 TM and Landsat 8 OLI Surface Reflectance (SR) images between 1996 and 2018 were acquired in GEE. Based on the cfmask band from SR collection, clouds and shadows in images were identified and we only chose the good quality images with clouds less than 10%. Besides, in order to reduce the influence of tidal inundation, the Normalized Difference Vegetation Index (NDVI) (Tucker, 1979) and Land Surface Water Index (LSWI) (Gao, 1996)

were calculated for mangrove samples to select the images with NDVI > LSWI, which has been applied for mapping rice paddy and mangroves (Zhou et al., 2016; Chen et al., 2017). Finally, the median of image collection for each year were used to supplement SAR data.

2.2.2 Ground-truth Data: Field surveys were carried out in Zhejiang province and Fujian province. Photos of mangrove forests and surroundings were taken, and their corresponding locations were recorded by handheld GPS. Besides, mangrove locations were also collected by literature review and Google Earth very high spatial resolution satellite images. All the ground-truth data were used to select the training and validation samples.

2.2.3 Other Data: Data from OpenStreetMap and administrative map of China were adopted to delineate the coastline. 30-m SRTM DEM data were used to mask out the regions that may not be suitable for mangrove planting.

2.3 Methods

The whole process (Figure 2) can be divided into two parts. One is to create the mangrove distribution map for 2018 by classification and the other is to detect the changes for the year 1996, 2007, and 2010 by combing image-to-image and image-to-map change detection methods. The classification was conducted in GEE platform while the change detection was completed in R studio. Before classification, we first determined the area where mangroves are likely to occur. A 10-km coastline buffer zone for both inland and sea sides was created. And as most mangroves are distributed in areas with an elevation between -5 m and 10 m above the mean sea level and a slope of less than 10^{o}(Chen et al., 2017), we masked the area with high elevation and steep slope. The results are displayed in Figure 1. Then four widely used indices were selected. They are NDVI, Enhanced Vegetation Index (EVI) (Huete et al., 1997), modified Normalized Difference Water Index (mNDWI) (Xu, 2006) and LSWI. Additionally, Jia et al. (2014) developed the Inundated Mangrove Forest Index (IMFI) to distinguish the inundated mangrove with sea water. Therefore, we finally calculated these five indices for Landsat images. ALOS PALSAR-2 was acquired with HH and HV bands while the JERS-1 was HH band alone. Additionally, we calculated the HH-HV and HH/HV for ALOS PALSAR-2 mosaics.

Figure 2 Flowchart of mangrove baseline mapping and change detecting

Based on the ground-truth data, we selected samples for mangrove and non_mangrove (seawater, agriculture, aquaculture, salt marsh and mudflat). 70% of the samples were randomly selected for training, and the remaining were used for validation. Then Random Forests (RF) Classifier was employed to classify the ALOS-Landsat stack in 2018. A measure of variable importance within the RF classifier revealed 6 bands (LSWI, NDVI, mNDWI, IMFI, HH, HH-HV) to be important to identify mangroves. Thus, these bands were used as input variables in a RF classifier. Finally, the mangrove distribution map in coastal China for 2018 was generated and the classification accuracies were calculated for each area.

Change detection in RS is usually achieved by image-to-image (Bruzzone and Prieto, 2000) or map-to-map (Dingle et al., 2011) approaches. Image-to-image method relies on identifying the objects by image enhancement while map-to-map method is based on the multi-date data classification. However, the image-to-image method would be influenced by the differences in image calibration and map-to-map method may suffer from error propagation. To overcome these limitations, Thomas et al. (2018) propose a new map-to-image method to detect changes, which used the base map to mask the image in other years and then got the normal distribution of the pixel values in masked area by removing the changed pixels. This method has been proved to be effective to detect the changes in mangrove forests. However, it doesn't work when the mangrove areas are small, or the changes are not obvious. The mangrove distribution in China is relatively sparse, thus, it is necessary to improve this method to make it more applicable in China. In this study, we combined the map-to-image method with image-to-image method to detect the changes of mangroves in China. Firstly, we used the mangrove map in 2018 which we got before to mask the ALOS-Landsat stacks for 1996, 2007 and 2010. Then the masked images were subtracted by the images in 2018 to produce new images which represent the change between two years. Two subtracted images were created for NDVI, LSWI and

HH band respectively. A series of threshold values for NDVI, LSWI and HH based on the mean differences between mangrove and other classes were used on the new image to determine the changed from unchanged pixels. The changed pixels were defined as the loss of mangrove while the unchanged pixels were the remaining mangrove. What's more, a 1000-m buffer were created to detect the gain of mangrove, which may occur at outside the mask area. The changed pixels in buffer area were reclassified into mangrove and non_mangrove. The new mangrove pixels were regarded as gains of mangrove.

3. RESULTS

The mangrove distribution map over China in 2018 was displayed in Figure 3. A total of 26,553 ha of mangroves were classified across 5 coastal provinces, Hong Kong, Macao and Taiwan, ranging from 10.62 ha in Macao to 10,853.46 ha in Guangdong province (Table 1). The accuracies for most areas were over 90% between 88.89% (Zhejiang) and 99.02% (Hong Kong). The overall accuracy for the whole region was 96.03%, with a kappa coefficient of 0.8858.

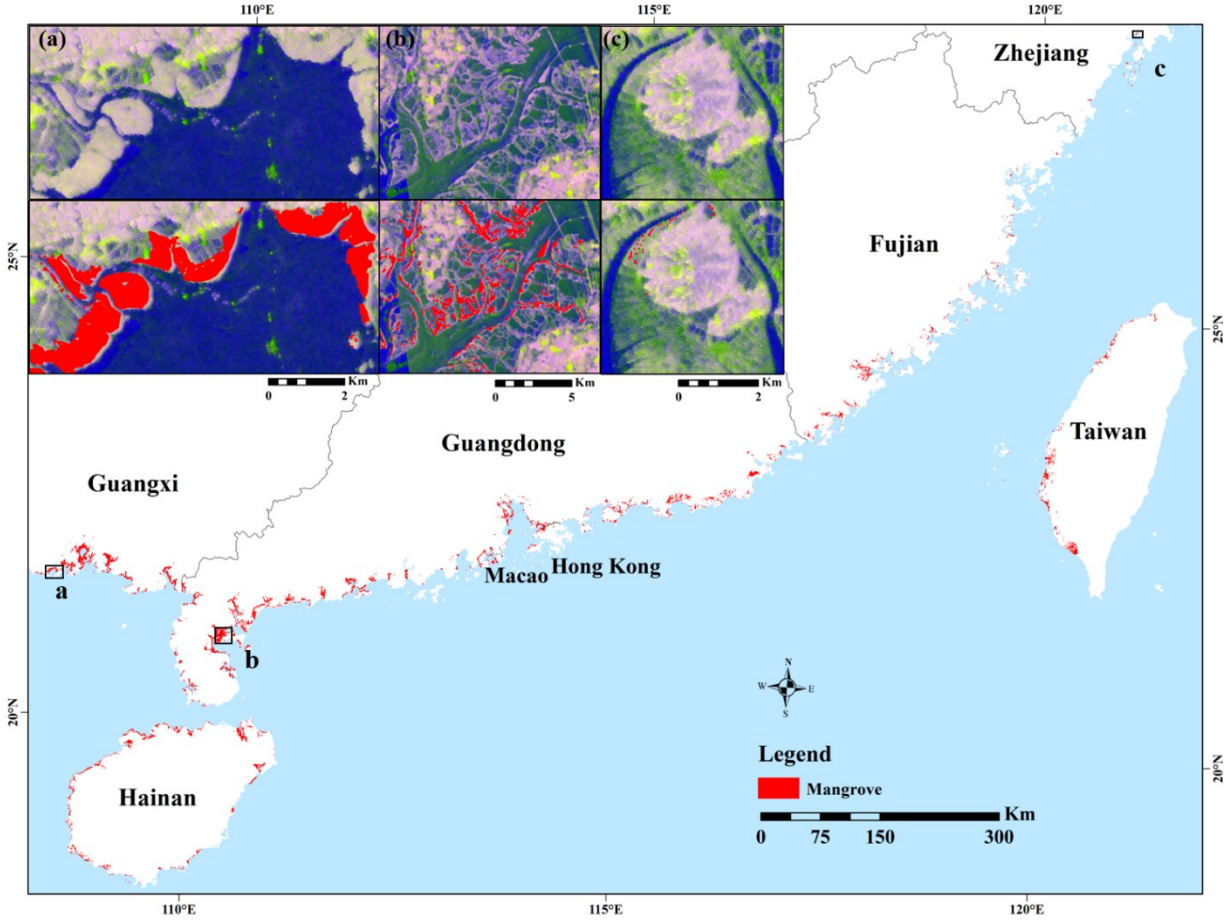

Figure 3 Spatial distribution of China's mangroves in 2018 and zoom views of three mangrove natural reserves: (a) Guangxi Beilun Estuary National Nature Reserve; (b) Zhanjiang Mangrove National Nature Reserve; and (c) Zhejiang Ximen Island Marine Special Reserve. The background of (a)-(c) are ALOS PALSAR-2 mosaic in 2018 shown in R: G: B = HH: HV: HH-HV composite.

Table 1 Classification results and accuracy assessments for each province (district)

Province	Area (ha)	Producer accuracy (%)	User accuracy (%)	Overall accuracy (%)	Kappa coefficient
Zhejiang	24.48	80.28	81.80	88.89	0.6200
Fujian	908.55	96.92	98.06	98.76	0.9496
Guangdong	10,853.46	94.88	95.56	96.22	0.9042
Guangxi	9,410.76	97.30	98.47	98.30	0.9571
Hainan	4,269.78	93.17	93.36	93.25	0.8646
Hong Kong	533.34	98.89	99.06	99.02	0.9794
Macao	10.62	-	-	-	-
Taiwan	542.34	87.72	94.52	93.83	0.8115
Total	26,553.33	-	-	96.03	0.8858

Note: accuracy was not calculated in Macao due to the limited samples.

The mangrove area changes for each area over the period 1996-2018, 2007-2018 and 2010-2018 were shown in Table 2 and the mangrove areas for each area in 1996, 2007, 2010 and 2018 were displayed in Figure 4. Over the period 1996-2010 mangroves in China experienced a net gain of 7133 ha and the areas for 1996, 2007 and 2010 were 19,420 ha, 24,684 ha and 25,573 ha respectively. Most mangroves were distributed in Guangdong, Guangxi and Hainan which contributed to more than 90% of the total area. Mangrove areas in Guangdong, Guangxi, and Hong Kong kept increasing during the past 20 years, while mangroves in Zhejiang kept decreasing at the same time period. Mangroves areas in Fujian, Hainan, Macao and Taiwan experienced a net gain firstly and then a net loss. The largest change observed was in Guangdong where 4,249.35 ha of mangrove gain occurred between 1996 and 2018. The smallest changes were observed at Macao, where 1.08 ha of mangrove loss was observed between 2010 and 2018. Since 2010, the mangrove areas have been relatively stable compared with before.

4. DISCUSSIONS

4.1 Base Map Classification

In this study, the mangrove baseline over China in 2018 was created by combining ALOS PALSAR and Landsat images. The method successfully mapped mangrove extent by reducing the influence of clouds and tides. This method was able to achieve an overall accuracy in excess of 95% and a kappa coefficient of 0.8858. The accuracy of the mangrove baseline at Zhejiang was less than 90% due to the similar spectral information between planted mangroves and salt marshes. However, its accuracy in excess of 80% represents the map of sufficient quality for use within the research community and policy making. Comparing with the existing national mangrove maps, the mangrove areas (26,553 ha) generated from this baseline was greater than others (Chen et al., 2017: 20,303 ha; Jia et al., 2018: 22,419ha). One reason is that they got the mangrove areas in 2015 which may be changed in the next 3 years. Besides, they used the Landsat imagery alone which would be influenced by clouds. The combination of optical and SAR data in this study provided the comprehensive and different information for the whole study area without the influence of clouds. Furthermore, optical imagery was able to provide information on the chemical and biophysical composition of the land covers while SAR data provided more information on their structure. This could help identify the mangrove with other coastal vegetations. Previous researches have revealed that there was a 20% increase in accuracy by combining optical and SAR datasets than using them independently (Ramsey et al., 1998; Held et al., 2003), although the combination of optical and SAR has received little attention for mangrove mapping, especially in China. The causes of error within the base maps were mainly caused by the tidal influences and spectral similarity of vegetations, particularly where other coastal wetlands adjoined mangroves. For example, in Zhejiang province, the planted mangroves were much shorter than the natural species with only around1-m height and distributed sparsely. These characteristics makes them more susceptible to the tidal inundation. Although we select the Landsat images in low tide period, we can't ensure the SAR image is in low tide period since there is only one SAR mosaic each year. As we can see in Figure 3(a)-(c), it is more difficult to identify the mangroves in Zhejiang province by visual interpretation compared with other two provinces. Thus, the lower classification accuracy in Zhejiang province is probably due to the influence of tides on SAR image. Besides, Zhejiang province has a large area of salt marshes, such as about 2432-ha *Spartina alterniflora* (Wang et al., 2015). Salt marshes usually distributed in adjacent areas of mangroves as shown in Figure 3(c), which have similar spectral information with mangrove especially in high tide period. So, it is hard to distinguish them without enough ground-truth data or very high-resolution images. Despite this, the accuracy of the baseline in each region ensure that they are suitable for informing both local and regional management strategies, whilst satisfying the requirements for national initiatives, including "Blue Carbon Project".

Table 2 Mangrove area changes for each province (district) in 1996, 2007 and 2010 compared with 2018

Province	1996			2007			2010		
	Gain (ha)	Loss (ha)	Net (ha)	Gain (ha)	Loss (ha)	Net (ha)	Gain (ha)	Loss (ha)	Net (ha)
Zhejiang	17.91	0.54	17.37	48.15	14.67	33.48	28.35	12.69	15.66
Fujian	91.17	333.9	-242.73	219.60	243.99	-24.39	259.74	168.21	91.53
Guangdong	64.44	4,313.79	-4,249.35	58.95	995.94	-936.99	26.10	499.14	-473.04
Guangxi	75.42	2,052.90	-1,977.48	65.25	911.25	-846	25.92	628.38	-602.46
Hainan	47.61	568.89	-521.28	94.95	162.72	-67.77	95.22	92.34	2.88
Hong Kong	0.45	94.41	-93.96	0.09	31.77	-31.68	2.25	12.96	-10.71
Macao	0.45	6.3	-5.85	0.18	2.25	-2.07	2.07	0.99	1.08
Taiwan	7.29	67.68	-60.39	22.32	15.93	6.39	3.60	8.91	-5.31
Total	304.74	7,438.41	-7,133.67	509.49	2,378.52	-1,869.03	443.25	1,423.62	-980.37

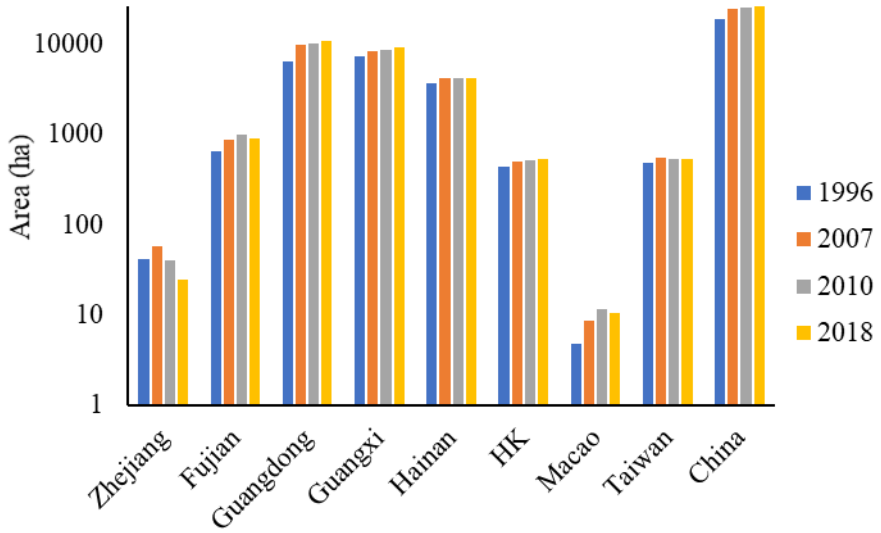

Figure 4 Mangrove area changes for each province (district) and the whole coastal zone in China

4.2 Change Detection

Mangroves changes were detected using a combination of map-to-image and image-to-image methods. These methods enhanced the detection of change features between images 11acquired in different years and avoid the error propagation caused by different classification results in different images. Furthermore, it is not limited to a certain mangrove area and thus, has a wide applicability in the field of change detection. However, the threshold values for detecting changed pixels may influence the accuracies. In this study, we calculated the mean differences between mangroves and other classes and then chose the minimum difference as the threshold to detect changes. In most cases, it worked, but the mean differences can only represent the average changes. Thus, there were some errors in the detection process which would be improved by further modification.

Our results demonstrate that mangroves in China have a tendency of gain between 1996 and 2018. According to literature reviews and field surveys, these gains were strongly associated with the national conservation actions. Since the early 1990s, China's government has published a number of laws and regulations to protect mangrove ecosystems, including the Action Plan for China Biodiversity Protection (State Environmental Protection Agency, 1994), the Forestry Action Plan for China's Agenda of the 21st Century (State Forestry Administration, 1995; 1996), the Plan for China Ecological Environment Conservation (The State Council, 1998), and the Action Plan for China Wetland Protection (State Forestry Administration, 2000) and so on. Under these laws and regulations, many mangrove reserves have been established which contributed to the reforestation of large-scale mangroves.

4.3 Future Work

This study provided the datasets of current mangrove distributions in China and their changes in the past 20 years. However, there are more work need to be done to help protect and recover mangrove ecosystems. Firstly, more details about the changes should be obtained, such as the changes in landward and seaward boundaries of mangrove ecosystems and the biomass changes. Then, according to the changes, quantitatively analysis can be conducted to evaluate the vulnerability of mangrove ecosystems to both climate change and human activities. Finally, suitable areas for recovering mangrove and exiting mangroves which need to be protected in the future would be found.

5. CONCLUSION

This study updates the mangrove baseline over China in 2018 by combining ALOS PALSAR and Landsat datasets with an accuracy greater than 95%. A novel combination of map-to-image method and image-to-image method was used to detect the changes in mangrove extent based on NDVI, LSWI and HH band in each year. The approach outlines a method that can detect the small changes in mangroves. The total areas of China's mangroves in 1996, 2007, 2010 and 2018 were 19,420 ha, 24,684 ha, 25,572 ha and 26,553 ha respectively. More than 90% mangroves were distributed in Guangdong province, Guangxi province and Hainan province. Mangroves in most areas kept increasing during the past 20 years due to the national conservation actions. It is important that mangrove changes are tied closely with additional ancillary data on the provision of ecosystem services. Thus, it is necessary to evaluate the vulnerability of mangrove ecosystems to climate change and human activities for future protection and reforestation.

REFERENCES

Arkema, K.K., Guannel, G., Verutes, G., Wood, S.A., Guerry, A., Ruckelshaus, M., Kareiva, P., Lacayo, M. and Silver, J.M., 2013. Coastal habitats shield people and property from sea-level rise and storms. Nature Climate Change, 3(10), p.913.

Bruzzone, L. and Prieto, D.F., 2000. Automatic analysis of the difference image for unsupervised change detection. IEEE Transactions on Geoscience and Remote sensing, 38(3), pp.1171-1182.

Chen, B., et al., 2017. A mangrove forest map of China in 2015: Analysis of time series Landsat 7/8 and Sentinel-1A imagery in Google Earth Engine cloud computing platform. ISPRS Journal of Photogrammetry and Remote Sensing, 131, pp. 104-120.

Chen, L., et al., 2009. Recent progresses in mangrove conservation, restoration and research in China. Journal of Plant Ecology, 2(2), pp. 45-54.

Dingle Robertson, L. and King, D.J., 2011. Comparison of pixel-and object-based classification in land cover change mapping. International Journal of Remote Sensing, 32(6), pp.1505-1529.

Duarte, C M., et al., 2013. The role of coastal plant communities for climate change mitigation and adaptation. Nature Climate Change, 3(11), pp. 961.

Gao, B., 1996. NDWI—A normalized difference water index for remote sensing of vegetation liquid water from space. Remote Sensing of Environment, 58(3), pp. 257-266.

Giri, C., et al., 2011. Status and distribution of mangrove forests of the world using earth observation satellite data. Global Ecology and Biogeography, 20(1), pp. 154-159.

Hamilton, S E. and CASEY, D., 2016. Creation of a high spatio-temporal resolution global database of continuous mangrove forest cover for the 21st century (CGMFC-21). Global Ecology and Biogeography, 25(6), pp. 729-738.
He, Y. and Zhang, M.X., 2001. Study on wetland loss and its reasons in China. Chinese Geographical Science, 11(3), pp.241-245.
Held, A., Ticehurst, C., Lymburner, L. and Williams, N., 2003. High resolution mapping of tropical mangrove ecosystems using hyperspectral and radar remote sensing. International Journal of Remote Sensing, 24(13), pp.2739-2759.
Hu, L., Li, W., Xu, B., 2018. Monitoring mangrove forest change in China from 1990 to 2015 using Landsat-derived spectral-temporal variability metrics. International journal of applied earth observation and geoinformation, 73, pp. 88-98.
Huete, A R., et al., 1997. A comparison of vegetation indices over a global set of TM images for EOS-MODIS. Remote Sensing of Environment, 59(3), pp. 440-451.
Jia, M., et al., 2014. Mapping China's mangroves based on an object-oriented classification of Landsat imagery. Wetlands, 34(2), pp. 277-283.
Jia, M., Wang, Z., Zhang, Y., Mao, D. and Wang, C., 2018. Monitoring loss and recovery of mangrove forests during 42 years: The achievements of mangrove conservation in China. International journal of applied earth observation and geoinformation, 73, pp.535-545.
Lee, J.S., 1980. Digital image enhancement and noise filtering by use of local statistics. IEEE Transactions on Pattern Analysis & Machine Intelligence, (2), pp.165-168.
Murray, B.C., Pendleton, L., Jenkins, W.A. and Sifleet, S., 2011. Green payments for blue carbon: economic incentives for protecting threatened coastal habitats. Green payments for blue carbon: economic incentives for protecting threatened coastal habitats.
Nagelkerken, I., Van der Velde, G., Gorissen, M.W., Meijer, G.J., Van't Hof, T. and Den Hartog, C., 2000. Importance of mangroves, seagrass beds and the shallow coral reef as a nursery for important coral reef fishes, using a visual census technique. Estuarine, coastal and shelf science, 51(1), pp.31-44.
Ramsey, E.W., Nelson, G.A. and Sapkota, S.K., 1998. Classifying coastal resources by integrating optical and radar imagery and color infrared photography. Mangroves and Salt Marshes, 2(2), pp.109-119.
Spalding, M D., Blasco, F., Field, C D., 1997. World mangrove atlas.
Spalding, M., Kainuma, M., Collins, L., 2010. World atlas of mangroves. A collaborative project of ITTO, ISME, FAO, UNEP-WCMC.
Thomas, N., Bunting, P., Lucas, R., Hardy, A., Rosenqvist, A. and Fatoyinbo, T., 2018. Mapping mangrove extent and change: A globally applicable approach. Remote Sensing, 10(9), p.1466.
Tucker, C J., 1979. Red and photographic infrared linear combinations for monitoring vegetation. Remote Sensing of Environment, 8(2), pp. 127-150.
Wang, A., Chen, J., Jing, C., Ye, G., Wu, J., Huang, Z. and Zhou, C., 2015. Monitoring the invasion of Spartina alterniflora from 1993 to 2014 with Landsat TM and SPOT 6 satellite data in Yueqing Bay, China. PLoS One, 10(8), p.e0135538.
Wang W.Q. Chinese Mangrove Science Press, Beijing, China (2007)
Wu, P Q., et al., 2013. Remote sensing monitoring and analysis of the changes of mangrove resources in China in the past 20 years. Adv. Mar. Sci, 31, pp. 406-414.
Xu, H., 2006. Modification of normalised difference water index (NDWI) to enhance open water features in remotely sensed imagery. International Journal of Remote Sensing, 27(14), pp. 3025-3033.
Zhou, Y., Xiao, X., Qin, Y., Dong, J., Zhang, G., Kou, W., Jin, C., Wang, J. and Li, X., 2016. Mapping paddy rice planting area in rice-wetland coexistent areas through analysis of Landsat 8 OLI and MODIS images. International journal of applied earth observation and geoinformation, 46, pp.1-12.